Publications of the Astronomical Society of the Pacific, **117**:810–822, 2005 August

An Atlas of Spectrophotometric Landolt Standard Stars

Maximilian Stritzinger,[1,2] Nicholas B. Suntzeff,[3] Mario Hamuy,[4] Peter Challis,[5] Ricardo Demarco,[6] Lisa Germany,[7] and A. M. Soderberg[8]

Received 2005 April 11; accepted 2005 May 2; published 2005 July 6

ABSTRACT. We present CCD observations of 102 Landolt standard stars obtained with the Ritchey-Chrétien spectrograph on the Cerro Tololo Inter-American Observatory 1.5 m telescope. Using stellar atmosphere models, we have extended the flux points to our six spectrophotometric secondary standards, in both the blue and the red, allowing us to produce flux-calibrated spectra that span a wavelength range from 3050 Å to 1.1 μm. Mean differences between *UBVRI* spectrophotometry computed using Bessell's standard passbands and Landolt's published photometry were determined to be 1% or less. Observers in both hemispheres will find these spectra useful for flux-calibrating spectra, and through the use of accurately constructed instrumental passbands, will be able to compute accurate corrections to bring instrumental magnitudes to any desired standard photometric system (*S*-corrections). In addition, by combining empirical and modeled spectra of the Sun, Sirius, and Vega, we calculate and compare synthetic photometry to observed photometry taken from the literature for these three stars.

Online material: color figures, extended table

1. INTRODUCTION

From dedicated follow-up observations of supernovae (SNe), it has become clear that systematic magnitude differences can exist between data sets obtained at different telescopes for the same event. These differences can be on the order of several hundredths of a magnitude or more near maximum light, and potentially larger for late-time photometry when the spectrum enters the nebular phase. This effect is caused by the inexact match of filter sets employed at different telescopes (Suntzeff et al. 1988; Menzies 1989; Hamuy et al. 1990; Suntzeff 2000), and is magnified when the instrumental filters differ grossly from the standard Johnson/Kron-Cousins passbands. Although the observed photometry is standardized to a common system through the use of color terms, this is not expected to work perfectly, because there are radical differences between the normal and continuous spectral energy distributions (SEDs) of the photometric standard stars compared to the SEDs of SNe, which are dominated by strong absorption and emission features.

Using SN photometry uncorrected for this effect can lead to incorrect calculations of colors, host galaxy reddening, absolute magnitudes, and can ultimately bias cosmological parameters. However, the photometrist can remedy this by computing "*S*-corrections" to correct the photometry to a standard filter transmissivity function. An at least partially successful attempt to reconcile these magnitude differences in the optical for the well-observed SN 1999ee was made by Stritzinger et al. (2002). More recently, this photometric technique has been used in the optical and extended to near-infrared photometry by Krisciunas et al. (2003, 2004), Candia et al. (2003), and Pignata et al. (2004) for a number of other well-observed SNe.

Spectrophotometric standard stars play a crucial role in determining accurate *S*-corrections. However, there exists only a small number of moderately faint standard stars—which are of limited color range—useful for spectroscopic calibrations. In this work we construct a large atlas of flux-calibrated spectra in order to enlarge the hitherto available spectrophotometric standards. Our program consists of a large number of Landolt standard stars (~100) that have well-documented photometric magnitudes and are widely used for photometric calibrations. These standard stars can now be employed to flux-calibrate spectra necessary for determining many physical parameters of stars (e.g., surface temperatures, radial velocities, abundances, surface gravities, etc.), relate spectral and photometric observations, and to calculate *UBVRIz*-band *S*-corrections for any celestial object whose SED significantly differs from the stan-

[1] Max-Planck-Institut für Astrophysik, Karl-Schwarzschild-Strasse 1, 85741 Garching, Germany; stritzin@mpa-garching.mpg.de.

[2] Visiting Astronomer, Cerro Tololo Inter-American Observatory.

[3] Cerro Tololo Inter-American Observatory, Casilla 603, La Serena, Chile; nsuntzeff@noao.edu.

[4] Las Campanas Observatory, Carnegie Observatories, Casilla 601, La Serena, Chile; mhamuy@lco.cl.

[5] Harvard-Smithsonian Center for Astrophysics, 60 Garden Street, Cambridge, MA 02138; pchallis@cfa.harvard.edu.

[6] Department of Physics and Astronomy, Johns Hopkins University, 3400 North Charles Street, Baltimore, MD 21218; demarco@pha.jhu.edu.

[7] European Southern Observatory, Alonso de Cordova 3107, Vitacura Santiago, Chile; lgermany@eso.org.

[8] California Institute of Technology, 1201 East California Boulevard, Pasadena, CA 91125; ams@astro.caltech.edu.

dards used to calibrate the observed photometry. These spectra are now available for other researchers.[9]

The motivation for the present study was to be able to model a typical night's run of photometry at a facility telescope and CCD instrument. We would like to be able to start with the SEDs of the program objects, usually SNe, and the Landolt stars. Then with system transmission functions, which include atmospheric extinction, mirror reflectivities, filter functions, Dewar windows, and the detector quantum efficiencies, we should be able to calculate synthetic magnitudes as close as possible to the observed natural system. Finally, we want to use the synthetic natural system magnitudes and run them through our photometric codes to calculate the typical extinction and color terms that are solved for each night. By comparing the synthetic to the observed transformations, we can assess the effects of many possible systematic errors in our data. How closely do the color terms match: How does the changing extinction across the photometric bands affect the calculated colors at higher air mass? It should also be possible, in principle, to calculate the transmission functions of the photometric bands from scratch using the observed photometric solutions and the SEDs (Jha 2002). Jha modeled the transmission curves with cubic splines spaced equally over the wavelength region in which a nonzero response was expected in the *UBVRI* bands. Typically six to eight spline points were used in each band, with the first and last points forced to zero at wavelengths expected to have zero transmissivity slightly outside the expected passbands. Roughly 20 spectrophotometric standards with well-established *UBVRI* magnitudes were used in creating the synthetic magnitudes and were observed with the filter system in his study. A best-fit model transmission function in each filter was made by minimizing the residuals between the synthetic and observed magnitudes. The model fits the amplitudes of the spline points restricted to values between zero and 1. Jha noted that the model functions reproduce the transmission functions measured in the lab reasonably well. Increasing the number of standards observed would improve the fits and possibly allow more spline knots to be used.

As an example (which may surprise most astronomers who do not do photometry) very few photometrists use second-order (color dependent) terms in the extinction, because it is difficult to measure this effect accurately. Most extinction is handled as a simple grayshift of the form $m(\mathrm{nat})_0 = m(\mathrm{nat}) - kX$, where X is the extinction and k is the extinction coefficient of a given bandpass. The extinction curve is included in our system throughput curves when doing synthetic photometry, but we do not gauge its effects on the color for stars observed at $X = 1$ versus $X = 2$. With this atlas of Landolt SED spectra, it is now possible to calculate the second-order terms using synthetic photometry.

The structure of this paper is as follows. In § 2 we present our observations, followed by the spectroscopic reductions in § 3. Our results for the program stars are given in § 4.1. Finally, in § 4.2 synthetic photometry of the Sun, Sirius, and Vega is computed and compared to observed magnitudes found in the literature.

2. OBSERVATIONS

Six bright ($4.3 \lesssim V \lesssim 5.7$) secondary standard stars (see Table 1) originally published in Hayes (1970) and later recalibrated by Taylor (1984) and Hamuy et al. (1992, 1994) were adopted as our defining spectrophotometric system. These stars are secondary standards because they tie the Kitt Peak National Observatory and Cerro Tololo Inter-American Observatory (CTIO)[10] spectrophotometric standards (Massey et al. 1988; Hamuy et al. 1992, 1994) to Vega. The program consists of 102 Landolt standard stars located along the celestial equator, in the range $7.0 \lesssim V \lesssim 13.0$. The reader is referred to Landolt (1983, 1992a, 1992b) and Hamuy et al. (1992) and references therein for spectral classifications, *UBVRI*-band photometry, coordinates, and finding charts. The reference and observed photometry for each star can also be found in the image header of each spectrum.

All observations were obtained with the CTIO 1.5 m telescope, using the Ritchey-Chrétien (R-C) spectrograph, during 1999 February 5–13 (UT). Of the eight nights observed, all were photometric, except the last night, 1999 February 12–13 (UT). Half of the observations were dedicated to a blue setup, while the other half were allocated to a red setup. The blue setup employed a low-dispersion grating (300 lines mm^{-1}) with a dispersion of 2.85 Å pixel^{-1} blazed at 4000 Å and a 1200 × 800 LORAL CCD. We observed in first order, with a total wavelength coverage of 3300 Å (3100–6400 Å) and a FWHM resolution of 8.6 Å. The red setup consisted of a low-dispersion grating (158 lines mm^{-1}) with a dispersion of 5.34 Å per pixel blazed at 8000 Å with the same LORAL CCD. We observed in first order, with a total wavelength coverage of 4800 Å (5800–10600 Å) and a FWHM resolution of 16.4 Å. An OG570 second-order blocking filter was used to suppress any leakage, which otherwise would have contaminated the spectra redward of 6000 Å.

Daily observations began by obtaining calibration images. This included bias frames, dome flats with a 2″ and 21″ slit, and finally twilight flats through a 21″ slit. On nights in which we observed with the blue setup, projector flats were taken with a quartz lamp. With the projector flats, we used $CuS0_4$ and Corning 9863 filters to prevent saturation of the CCD. The observing procedure consisted of (1) pointing the telescope to the coordinates of the standard star, (2) closing the slit to 2″ and then taking an exposure with a HeAr lamp, (3) selecting

[9] The data are provided in electronic form as FITS files; see http://csp1.lco.cl/~mhamuy/SPECSTDS.

[10] Cerro Tololo Inter-American Observatory, Kitt Peak National Observatory, National Optical Astronomy Observatories, operated by the Association of Universities for Research in Astronomy, Inc., (AURA), under cooperative agreement with the National Science Foundation.

TABLE 1
SPECTROPHOTOMETRIC SECONDARY STANDARDS

λ (Å)	Δλ	HR 718	HR 1544	HR 3454	HR 4468	HR 4963	HR 5501
3100	45	5.265	5.634	4.080	5.581	5.669	6.737
3150	45	5.256	5.611	4.099	5.576	5.653	6.731
3200	45	5.243	5.589	4.109	5.567	5.637	6.726
3250	45	5.230	5.566	4.125	5.557	5.618	6.717
3300	25	5.218	5.542	4.135	5.552	5.601	6.712
3390	45	5.188	5.519	4.145	5.530	5.563	6.675
3448	45	5.185	5.498	4.168	5.519	5.544	6.667
3509	45	5.175	5.485	4.185	5.517	5.519	6.654
3571	45	5.155	5.466	4.203	5.502	5.499	6.639
3636	45	5.117	5.422	4.197	5.474	5.451	6.608
4036	45	3.930	4.065	3.822	4.337	4.084	5.373
4167	45	3.983	4.110	3.892	4.383	4.123	5.410
4255	45	4.006	4.123	3.916	4.409	4.144	5.427
4464	45	...	4.160	3.983	4.461	4.181	5.476
4566	45	4.091	4.194	4.034	4.502	4.224	5.510
4785	45	4.134	4.222	4.104	4.545	4.247	5.551
5000	45	4.182	4.274	4.175	4.592	4.290	5.587
5264	45	4.235	4.322	4.239	4.653	4.339	5.638
5556	45	4.291	4.363	4.318	4.713	4.376	5.689
5840	45	4.336	4.403	4.388	4.770	4.422	5.738
6058	45	4.393	4.452	4.460	4.822	4.474	5.791
6440	45	4.465	4.516	4.544	4.902	4.543	5.846
6792	45	4.532	4.562	4.623	4.961	4.590	5.889
7102	45	4.593	4.616	4.709	5.019	4.646	5.952
7554	45	4.678	4.693	4.797	5.104	4.718	6.031
7845	45	4.740	4.745	4.861	5.168	4.779	6.065
8092	45	4.766	4.763	4.912	5.194	4.796	6.099
8376	45	4.829	4.825	4.986	5.253	4.847	6.147
8800	10	4.824	4.850	5.039	5.287	4.843	6.177
8920	10	4.827	4.854	5.058	5.298	4.847	6.185
9915	45	4.862	4.867	5.193	5.354	4.888	6.225
9970	45	4.867	4.871	5.202	5.358	4.893	6.231
10150	45	4.891	4.882	5.234	5.378	4.919	6.251
10256	45	4.944	4.898	5.261	5.378	4.926	6.240
10406	45	4.968	4.914	5.296	5.414	4.960	6.271
10500	45	4.986	4.944	5.319	5.443	5.004	6.333
10600	45	5.022	4.965	5.351	5.469	5.041	6.366

NOTE.—All values are in monochromatic magnitudes $m_\nu = -2.5 \log_{10}(f_\nu) - 48.590$.

a random field star for telescope guiding purposes, and (4) taking an exposure of the standard star with a slit width of 21″.

On the first two nights, the secondary standards were each observed at three slit positions, and the program stars at two slit positions. By the third night, *all* stars were observed with four slit positions.[11]

For each night, typically five or six secondary standard stars were observed (see Table 1), obtaining between 50 and 70 spectra at a wide range of air mass between $X = 1.0$ and 2.3, in order to solve for the nightly extinction curve. When observing the program stars, we restricted the range of air mass to between $X = 1.0$ and 1.3, in order to reduce the differential effects of the Earth's atmosphere, such as telluric absorption and atmospheric refraction between the program and spectrophotometric standard stars. Integration times were chosen such that for the majority of one-dimensional spectra (resulting from adding all the flux in the two-dimensional image along the spatial direction), the number of counts was between 40,000 and 50,000 ADU per resolution element. For all observations, the predicted gain of the LORAL CCD was 1.420 detected electrons per ADU. Exposure times for the bright secondary standards ranged between 2 and 7 s, while exposure times for the program stars typically ranged between 25 and 400 s. Due to the short integration times of the secondary standards, it proved necessary to apply a shutter correction to their spectra

[11] A preliminary data reduction showed that all of the spectra from 5800 to 7000 Å were choppy at the 2%–4% level. This choppiness was similar to broad-scale fringing, which is typically seen at wavelengths longward of 8000 Å. To alleviate this problem, the observing procedure was changed to observe all stars at four slit positions at lower flux levels in order to obtain similar total integration times. The co-added frames reduced the level of choppiness by half.

(see § 3 below). From multiple exposures taken with 1, 2, 3, 4, and 6 s exposure times on 1999 February 6–7 (UT), an additive mean shutter error for a 1 s exposure was determined to be -0.023 ± 0.010 s (s.d.).

3. SPECTROSCOPIC REDUCTIONS

Standard spectroscopic reduction techniques using IRAF[12] were performed to reduce the data. To begin, the overscan and bias was subtracted from all spectra, including the HeAr frames. With the blue setup, a flat-field image was constructed using a combination of dome flats (external illumination), projector flats (internal illumination), and sky flats. The projector flats provide illumination in the ultraviolet end of the CCD ($\lambda < 3800$ Å), the dome flats at redder wavelengths, and the sky flat permitted us to correct the dome and projector flats for uneven illumination along the slit. With the red setup, we only used dome and sky flats. The resulting flats (normalized along the dispersion axis) were divided into all of the observed spectra. Next, we extracted one-dimensional spectra from the two-dimensional flat-fielded images and dispersion-calibrated them to a linear wavelength scale using the HeAr calibrations frames that were taken before each exposure. Shutter corrections were then applied to all the secondary standards by multiplying a factor of

$$\frac{\mathrm{ET}}{\mathrm{ET} + \mathrm{ST}} \tag{1}$$

into each spectra, where ET is the requested exposure time in seconds and ST is the mean shutter error given in § 2.

If the program stars were to be used as spectrophotometric standards for calculating *U*- and *z*-band spectrophotometry, it proved necessary to extend the wavelength range of their spectra beyond the 3300–10406 Å range of the secondary standards. This was accomplished by fitting synthetic spectra modeled with appropriate physical parameters to each of our secondary standards, using R. Kurucz's stellar atmosphere code, which has been modified by W. Vacca and P. Massey.[13] Input parameters for this program include surface temperature, log *g*, and metallicity abundances. The output models of this program are in step sizes of 10 Å and have a FWHM resolution of ~6 Å. By extrapolating from the models, we obtained six new flux points. These included four flux points blueward of 3300 Å at 3250, 3200, 3150, and 3100 Å, and two flux points redward of 10406 Å at 10500 and 10600 Å. It was necessary to scale the models to the observed blue and red spectra by multiplication of an arbitrary constant. This constant was derived such that the modeled spectrum could reproduce the same values (up to two significant figures) as the flux points given in Table 5 of Hamuy et al. (1992). In addition, because two of the Hamuy et al. (1994) flux points were placed in regions of strong atmospheric contamination, they were removed. However, to account for this wavelength interval, we placed two additional flux points at 7845 and 9915 Å. Also, two new flux points were added at 9970 and 10150 Å. Because there are no flux points from 8376–9834 Å, we attempted to add two flux points in this interval at locations free of atmospheric and stellar absorption features, at 8800 and 8920 Å, each with a 10 Å bandwidth. Unfortunately, when deriving the nightly response curve, these flux points showed systematic residuals up to ~0.10 mag, compared to neighboring flux points, and were thus omitted.

Table 1 lists the recalibrated monochromatic magnitudes of our spectrophotometric secondary standards from 3100 to 10600 Å. These values are defined by

$$m_\nu = -2.5 \log_{10} (f_\nu) - \mathrm{ZP}, \tag{2}$$

where f_ν is the monochromatic flux in ergs cm^{-2} s^{-1} Hz^{-1}, and ZP is the zero point for the magnitude scale. The zero point of the monochromatic magnitude scale was chosen to be -48.590 (Massey et al. 1988). In order to allow the reader to easily compare the monochromatic magnitudes listed in Table 1 with those provided in Hamuy et al. (1992), we list them in units of m_ν. However, for the rest of the paper we work in units of f_λ rather than f_ν.

Before flux-calibrating the spectra, it is important to remove as much of the instrumental artifacts (such as fringing) and telluric absorption as possible. The most difficult signature to remove is the flat-fielding error, which introduces very high order variations in the continuum at the few percent level, due to the continuum-fitting algorithms used to take a flat-field lamp and "flatten" it with an IRAF task such as *response*. Typically we used a polynomial of an order of 20 to 30 to fit out the flat-field response. This will introduce wiggles with a period of roughly 150 Å or so, which are impossible to remove with a polynomial fit to the Hayes (1970) flux points, which are often more than 200 Å apart. In the region of 8000–9500 Å, the flux points are even more separated, and one cannot fit out these flat-fielding errors.

However, Bessell (1999), who noticed correlated errors in the Hamuy et al. (1994) spectrophotometric standards, has suggested an ingenious way of removing these flat-fielding errors. He proposed that the data be divided by a spectral flat, preferably with a spectrum of an astrophysical source that is close to a blackbody or is otherwise line-free. There is no such source, but there are some stars listed in his table, such as Feige 110 or VMa2, that are close to being a pure continuum source. Most of these stars were too faint for the 1.5 m, so we had to do the next best thing—use the division of an observed spectrum of a hot star with the model of the hot star. We used HR 3454, which was observed every night at an air mass of ~1.2. To construct the red spectral flat, we first made a theoretical spectrum using the

[12] The Image Reduction and Analysis Facility (IRAF) is distributed by the National Optical Astronomy Observatory, which is operated by AURA, Inc., under a cooperative agreement with the National Science Foundation.

[13] R. Kurucz's stellar atmosphere models can be downloaded from his Web site: http://kurucz.harvard.edu.

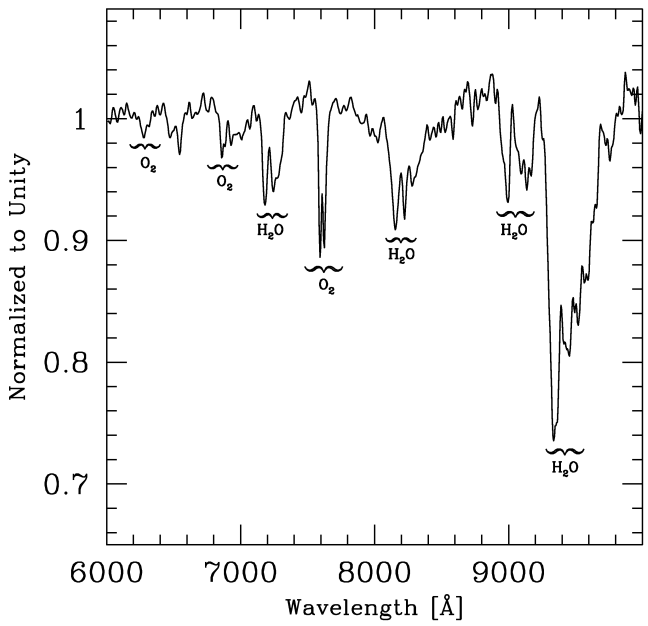

FIG. 1.—Plot of telluric features removed from all spectra by division of a spectral flat. This figure is the division of a high air-mass spectrum by an intermediate air-mass spectrum of HR 3454, normalized to unity. The more prominent telluric features are labeled.

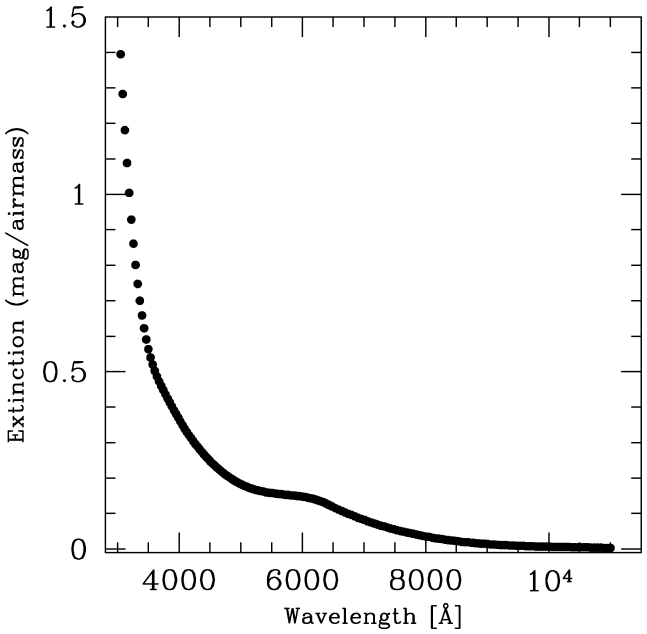

FIG. 2.—Averaged blue and red atmospheric extinction curves obtained at CTIO on 1999 February 5–12 (UT).

Kurucz code at the same dispersion and wavelength coverage as the observed spectra. Because the Kurucz models are only available for a large grid of physical parameters, it was necessary to interpolate from the models to produce a spectrum that most accurately matched HR 3454.[14] All the red dispersion-calibrated spectra of HR 3454 at an air mass of 1.2 were then averaged and divided by the modeled spectrum. A few of the strongest spectral features, such as Hα, did not cleanly disappear in the spectral flat. Therefore, these residuals were removed by interpolation. Next, all of the red dispersion-calibrated data for each night were divided by this spectral flat field. Figure 1 displays the main telluric features redward of 6000 Å that were removed from all the red spectra by the division of the spectral flat. The most prominent telluric features were those associated with atmospheric H_2O and O_2. The O_2 A and B bands were saturated for all observations, whereas the strength of the H_2O features were strongly dependent on both the air mass and the time at which the star was observed.

The blue spectral flat was constructed by averaging all the dispersion-calibrated observations of HR 3454 made at an air mass of 1.2. The blue spectral flat was then divided into all of the blue dispersion-calibrated data. Through the use of spectral flat fields, we obtained smooth dispersion-calibrated spectra free of large telluric absorption and instrumental features.

Next we proceeded to flux-calibrate the data using our fully reduced spectrophotometric secondary standards. Data from each night were first corrected for atmospheric extinction via the nightly extinction curves derived from the secondary spectrophotometric standards, which were observed to this end over a range of air masses. In Figure 2 we present an averaged extinction curve obtained from the seven photometric nights for both the blue and the red setups, and Table 2 lists this extinction curve in tabular form. To obtain flux-calibrated spectra, a nightly response curve was derived by fitting a low-order cubic spline to the observed flux values obtained from the secondary standards. When deriving nightly response curves, we were able to extend the wavelength range past our reddest flux point given in Table 1 by 400 Å to 11000 Å, and by 50 Å in the blue to 3050 Å. To calculate spectrophotometry for each star, it was necessary to stitch the blue and red spectra together. This was accomplished by first comparing all the blue and red spectra for an individual star at an air mass of 1.5 or less.

All of the spectra were combined by averaging them together (using the IRAF task *scombine* with the rejection option set to employ the averaged σ-clipping algorithm) to produce a master spectrum for each star. Each master spectrum covers a total wavelength range of 7950 Å (3050–11000 Å). When considering all of individual spectra together, the flux offsets were typically extremely small, on the order of ~0.001 mag.

An indication that the Bessell method of using spectral flats works well is that the flux-calibration curves were fitted with lower ordered polynomials. Without the division of the spectral flats, there would have been noticeable wiggles in the sensitivity curve, which would have required the use of high-order (12

[14] This spectrum corresponds to a model produced for physical parameters $T_{\rm eff}$ = 18,650 K, log g = 3.5, [M/H] = 0.

TABLE 2
AVERAGED EXTINCTION CURVE FOR CTIO

λ	Extinction (mag air mass^{-1})	λ	Extinction (mag air mass^{-1})	λ	Extinction (mag air mass^{-1})	λ	Extinction (mag air mass^{-1})
3050.00	1.395	4678.72	0.220	6307.43	0.134	8636.47	0.019
3084.65	1.283	4713.37	0.215	6342.09	0.132	8689.00	0.019
3119.31	1.181	4748.02	0.210	6376.74	0.129	8741.53	0.018
3153.96	1.088	4782.68	0.206	6411.39	0.126	8794.05	0.017
3188.61	1.004	4817.33	0.202	6446.05	0.123	8846.58	0.016
3223.27	0.929	4851.98	0.198	6480.70	0.120	8899.11	0.015
3257.92	0.861	4886.64	0.194	6482.85	0.120	8951.64	0.015
3292.57	0.801	4921.29	0.190	6535.38	0.115	9004.16	0.014
3327.23	0.748	4955.94	0.187	6587.91	0.111	9056.69	0.013
3361.88	0.700	4990.60	0.184	6640.44	0.107	9109.22	0.013
3396.54	0.659	5025.25	0.181	6692.96	0.103	9161.75	0.012
3431.19	0.623	5059.91	0.178	6745.49	0.099	9214.27	0.011
3465.84	0.591	5094.56	0.176	6798.02	0.096	9266.80	0.011
3500.50	0.564	5129.21	0.173	6850.55	0.092	9319.33	0.011
3535.15	0.540	5163.87	0.171	6903.07	0.088	9371.85	0.010
3569.80	0.520	5198.52	0.169	6955.60	0.085	9424.38	0.010
3604.46	0.502	5233.17	0.167	7008.13	0.082	9476.91	0.009
3639.11	0.487	5267.83	0.166	7060.65	0.078	9529.44	0.009
3673.76	0.473	5302.48	0.164	7113.18	0.075	9581.96	0.009
3708.42	0.460	5337.13	0.163	7165.71	0.072	9634.49	0.008
3743.07	0.448	5371.79	0.162	7218.24	0.069	9687.02	0.008
3777.72	0.436	5406.44	0.160	7270.76	0.066	9739.55	0.008
3812.38	0.425	5441.09	0.159	7323.29	0.064	9792.07	0.007
3847.03	0.414	5475.75	0.158	7375.82	0.061	9844.60	0.007
3881.69	0.402	5510.40	0.158	7428.35	0.058	9897.13	0.007
3916.34	0.391	5545.05	0.157	7480.87	0.056	9949.65	0.007
3950.99	0.381	5579.71	0.156	7533.40	0.053	10002.2	0.007
3985.65	0.370	5614.36	0.155	7585.93	0.051	10054.7	0.006
4020.30	0.360	5649.02	0.155	7638.45	0.049	10107.2	0.006
4054.95	0.349	5683.67	0.154	7690.98	0.047	10159.8	0.006
4089.61	0.339	5718.32	0.153	7743.51	0.045	10212.3	0.006
4124.26	0.330	5752.98	0.153	7796.04	0.043	10264.8	0.006
4158.91	0.321	5787.63	0.152	7848.56	0.041	10317.3	0.006
4193.57	0.313	5822.28	0.151	7901.09	0.039	10369.9	0.005
4228.22	0.304	5856.94	0.151	7953.62	0.037	10422.4	0.005
4262.87	0.296	5891.59	0.150	8006.15	0.035	10474.9	0.005
4297.53	0.289	5926.24	0.149	8058.67	0.034	10527.5	0.005
4332.18	0.281	5960.90	0.149	8111.20	0.032	10580.0	0.005
4366.83	0.274	5995.55	0.148	8163.73	0.030	10632.5	0.005
4401.49	0.267	6030.20	0.147	8216.25	0.029	10685.0	0.004
4436.14	0.260	6064.86	0.146	8268.78	0.028	10737.6	0.004
4470.79	0.254	6099.51	0.144	8321.31	0.026	10790.1	0.004
4505.45	0.247	6134.17	0.143	8373.84	0.025	10842.6	0.004
4540.10	0.241	6168.82	0.142	8426.36	0.024	10895.1	0.003
4574.76	0.236	6203.47	0.140	8478.89	0.023	10947.7	0.003
4609.41	0.230	6238.13	0.138	8531.42	0.022	11000.2	0.003
4644.06	0.225	6272.78	0.136	8583.95	0.020		

or so) polynomials. With the division of the spectral flats, we could use much lower polynomial fits. This gives us confidence that by using the spectral flats and fitting lower order polynomials, we have removed the systematic errors as seen by Bessell (1999) in the Hamuy et al. (1994) data.

4. RESULTS

4.1. Program Stars

In this section assess the spectrophotometric properties of our spectra by comparing broadband synthetic magnitudes to those measured by Landolt. As all objects were measured with a photon detector, a synthetic magnitude on the natural system must be calculated as the convolution of a star's photon flux N_λ with the filter instrumental passband $S(\lambda)$; i.e.,

$$\text{mag} = -2.5 \log_{10} \int N_\lambda S(\lambda)\ d\lambda + \text{ZP}, \qquad (3)$$

where ZP is the zero point for the magnitude scale. The variable

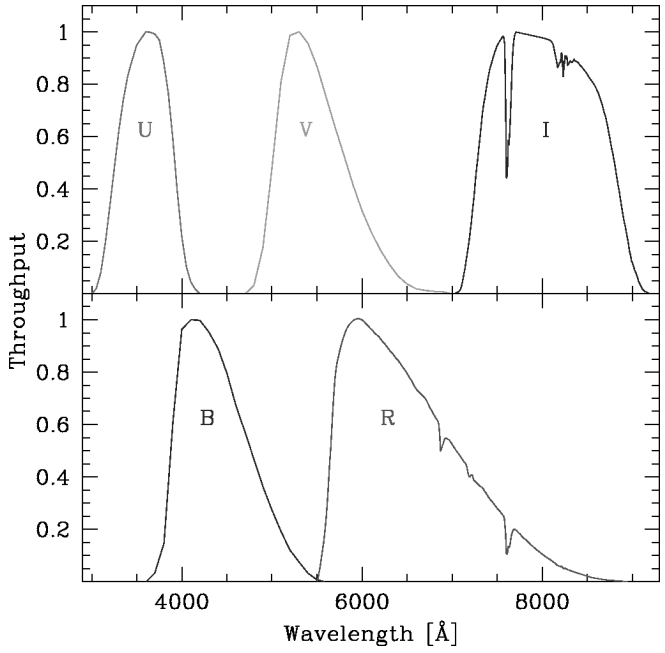

FIG. 3.—Johnson/Kron-Cousins *UBVRI* standard passbands from Bessell (1990). The Bessell transmission functions have been divided by λ for integrations with photon flux, and multiplied by an atmospheric line opacity spectrum, because they are used with spectra that have had telluric features removed. [*See the electronic edition of PASP for a color version of this figure.*]

$S(\lambda)$ should include the transparency of the Earth's atmosphere, the filter transmission, the quantum efficiency (QE) of the detector, and mirror reflectivities.

There is often confusion about the form of $S(\lambda)$. Some references use a function of the form $R(\lambda) = \lambda S(\lambda)$ and integrate $R(\lambda)F(\lambda)$, where $F(\lambda)$ is in units of ergs s^{-1} cm^{-2} $Å^{-1}$. In equation (3) we are specifying the photon flux in units of photons s^{-1} cm^{-2} $Å^{-1}$. With this definition, the meaning of $S(\lambda)$ is very easy to understand—it is just the fraction of photons (or energy) that is detected with respect to the incident flux outside the Earth's atmosphere. The variable $S(\lambda)$ accounts for all the flux lost due to the flux passing though the atmosphere, telescope, and instrument.

To construct the standard passbands, we adopted the Johnson/Kron-Cousins *UBVRI* transmission functions given in Bessell (1990; see our Fig. 3). Note, however, that the Bessell transmission functions are intended for use with energy rather than photon distributions (see Appendix in Bessell 1983). Thus, it was necessary to divide these functions by λ before employing them in equation (3) (Suntzeff et al. 1999; Hamuy et al. 2001). Because telluric absorption features were removed from the spectra, an atmospheric opacity spectrum was included in the construction of the standard passbands.

Armed with the standard passbands, we proceeded to calculate synthetic magnitudes for our spectra using zero points determined from secondary spectrophotometric standards (Landolt 1992b, 1999 private communication; Hamuy et al. 1994) rather than Vega, which has uncertain *UBVRI*-band optical photometry. When calculating zero points, we did not include telluric absorption in the passbands, because Hamuy et al. (1994) did not removed these features from their spectra. Table 3 lists the resulting zero points. Table 4 lists the synthetic magnitudes for all standard stars computed with equation (3) and the standard passbands, as well as the difference between observed and synthetic magnitudes. Note that the optical photometry for the secondary standards was taken from Hamuy et al. (1992). Sufficient wavelength coverage was obtained for 98 of the 108 standard stars listed in Table 4 to calculate *UBVRI* magnitudes. The remaining 10 stars were observed in either the blue or red, except HD 57884 and HD 60826, whose spectra were cut off blueward of 4000 Å. In Table 4 we also identify stars that are known or thought to be variable stars.

TABLE 3
ZERO POINTS EMPLOYED IN EQUATION (3) WITH STANDARD PASSBANDS

Filter	Zero Point
U	−14.244
B	−15.279
V	−14.850
R	−15.053
I	−14.556

In Figure 4 we present, for all standards observed, the difference between observed and synthetic magnitudes computed with the standard passbands, as a function of observed color. Overall, there is a high internal accuracy between the observed and synthetic magnitudes, as seen in Table 5, which lists the mean difference and associated standard deviation for each band. Mean differences between the observed photometry and our *UBVRI*-band synthetic magnitudes are 1% or less. However, it is evident from Figure 4 that slight color terms do exist, most notably in the *U*, *B*, and *R* bands. This color dependence reflects a small mismatch between the Bessell functions and the standards Johnson/Kron-Cousins system and/or a possible error in the fundamental spectrophotometric calibration. To remedy this problem, our approach consisted of applying wavelength shifts to the Bessell functions until we obtained a zero color dependence. Table 6 lists the resulting shifts. Although small compared to the Bessell bandwidths (~1000 Å), they have a non-negligible effect on the synthetic magnitudes, and the shifted standard passbands can be considered the best models for the Johnson/Kron-Cousins system. In Table 7 we provide our newly modeled *UBV* standard passbands. In Table 8 the *R* and *I* standard passbands are listed. Note that the *R* and *I* standard passbands include an atmospheric line opacity spectrum. In Figure 5 we present the comparison of Bessell's standard passbands (*dotted lines*) to our new modeled passbands (*dashed lines*). In addition, to complement the shifted passbands, we provide a convenient list of wavelength shifts (see Table 9)

TABLE 4
SYNTHETIC MAGNITUDES FOR ALL STARS

Star	U_{syn}	$U_{obs} - U_{syn}$	B_{syn}	$B_{obs} - B_{syn}$	V_{syn}	$V_{obs} - V_{syn}$	R_{syn}	$R_{obs} - R_{syn}$	I_{syn}	$I_{obs} - I_{syn}$
BD −0°454	11.849	+0.051	10.321	0	8.894	+0.001	8.152	−0.015	7.446	+0.004
BD +1°2447	12.318	+0.081	11.146	+0.015	9.634	+0.018	8.619	−0.011	7.380	+0.006
BD +5°1668[a]	12.597	+0.016	11.460	−0.060	9.906	−0.063	8.709	−0.072	7.116	+0.013
BD +5°2468	8.706	−0.034	9.242	−0.010	9.357	−0.009	9.383	+0.003	9.435	+0.005
BD +5°2529	12.001	+0.018	10.866	−0.035	9.584	−0.003	8.805	−0.005	8.125	+0.006
CD −32°9927	…	…	…	…	…	…	…	…	10.112	−0.005
EG 21	…	…	…	…	…	…	…	…	11.526	+0.004
G162-66	11.861	−0.010	12.873	−0.026	13.015	−0.003	13.126	+0.012	13.270	+0.008
HD 118246[b]	7.259	+0.053	7.895	+0.053	8.039	+0.050	8.098	+0.025	8.180	−0.010
HD 12021	8.413	−0.025	8.780	+0.012	8.872	+0.002	8.907	+0.009	8.972	0
HD 11983	…	…	…	…	…	…	…	…	6.627	+0.011
HD 121968	9.177	−0.017	10.081	−0.013	10.256	−0.002	10.319	+0.008	10.421	+0.005
HD 129975	11.741	+0.035	9.887	−0.010	8.370	+0.003	7.563	−0.019	6.769	−0.001
HD 16581	7.853	−0.020	8.131	+0.007	8.201	−0.006	8.220	0	8.254	+0.004
HD 21197	10.143	+0.014	9.046	−0.030	7.869	−0.003	7.191	−0.011	6.624	−0.004
HD 36395	10.616	+0.049	9.451	−0.017	7.969	−0.009	6.993	−0.018	5.877	+0.007
HD 47761[c]	8.207	+0.074	8.798	+0.085	8.648	+0.076	8.555	+0.031	8.469	−0.024
HD 50167	11.087	+0.053	9.402	−0.006	7.860	+0.001	7.043	−0.008	6.265	+0.013
HD 52533	6.655	+0.001	7.619	−0.005	7.702	0	7.706	+0.007	7.734	+0.006
HD 57884[c]	…	…	…	…	9.028	+0.107	7.821	+0.050	6.726	+0.122
HD 60826[c]	…	…	…	…	9.026	−0.043	7.544	−0.056	6.220	+0.086
HD 65079[a]	6.778	+0.086	7.615	+0.035	7.758	+0.074	7.763	+0.124	7.782	+0.180
HD 72055	7.555	−0.039	8.003	−0.027	8.125	−0.012	8.142	+0.002	8.187	+0.012
HD 76082	10.612	+0.005	9.553	−0.026	8.422	−0.013	7.851	−0.027	7.326	−0.018
HD 79097[b]	11.130	+0.032	9.214	+0.015	7.576	+0.025	6.613	−0.002	5.478	+0.036
HD 84971	7.742	−0.035	8.499	−0.022	8.650	−0.014	8.711	−0.012	8.804	−0.016
HD 97503	10.998	+0.003	9.910	−0.030	8.703	−0.001	7.993	−0.011	7.385	0
HR 0718	4.106	+0.010	4.209	+0.014	4.272	+0.007	4.294	+0.008	4.331	+0.011
HR 1544	4.372	−0.008	4.355	+0.010	4.349	+0.006	4.332	+0.009	4.322	−0.006
HR 3454	3.343	+0.009	4.096	−0.001	4.287	+0.008	4.368	+0.010	4.485	+0.010
HR 4468	4.459	−0.009	4.616	+0.014	4.691	+0.009	4.718	+0.005	4.746	+0.017
HR 4963	4.379	−0.014	4.358	+0.017	4.370	+0.005	4.364	+0.008	4.360	+0.005
HR 5501	5.585	−0.007	5.659	−0.001	5.685	−0.004	5.688	−0.011	5.694	+0.013
LTT 1788	13.349	−0.021	13.618	−0.007	…	…	…	…	…	…
LTT 2415	12.388	−0.016	12.604	−0.004	…	…	…	…	…	…
LTT 3218	…	…	…	…	…	…	…	…	11.646	−0.003
LTT 4364	…	…	…	…	…	…	…	…	11.189	−0.002
SA 94-305	11.876	+0.022	10.342	−0.030	8.910	−0.021	8.155	−0.023	7.455	−0.009
SA 94-308	9.229	+0.004	9.241	−0.004	8.754	−0.011	8.459	−0.006	8.177	−0.010
SA 94-342	10.706	+0.044	10.026	+0.008	9.035	+0.006	8.517	−0.003	8.019	+0.007
SA 95-52	10.145	+0.027	10.093	+0.010	9.571	+0.003	9.273	−0.006	8.971	−0.008
SA 95-96	10.234	−0.005	10.154	+0.003	10.022	−0.012	9.933	−0.002	9.835	+0.001
SA 95-132	12.776	+0.036	12.485	+0.027	12.057	+0.007	11.805	0	11.519	0
SA 95-206	9.259	−0.005	9.251	−0.012	8.748	−0.011	8.449	−0.002	8.162	0
SA 96-36	10.946	+0.010	10.836	+0.002	10.598	−0.007	10.469	−0.012	10.331	−0.010
SA 96-180[a]	10.875	−0.055	10.027	−0.048	8.957	−0.027	8.410	−0.028	7.892	−0.013
SA 96-235	13.097	+0.015	12.216	−0.002	11.145	−0.005	10.594	−0.013	10.069	+0.003
SA 96-393	10.283	+0.007	10.261	−0.013	9.659	−0.007	9.303	+0.004	8.960	+0.005
SA 96-406	9.656	+0.012	9.518	+0.002	9.306	−0.006	9.189	−0.005	9.068	−0.005
SA 96-737	14.191	+0.019	13.041	+0.009	11.717	−0.001	11.002	−0.019	10.298	−0.010
SA 97-249	12.487	−0.003	12.383	+0.003	11.737	−0.002	11.373	−0.004	11.021	−0.005
SA97-346	9.957	+0.011	9.863	−0.009	9.261	−0.001	8.916	+0.006	8.594	+0.004
SA 97-351	10.057	+0.022	9.978	+0.005	9.786	−0.005	9.653	+0.004	9.506	+0.011
SA 98-193	12.326	+0.036	11.206	+0.004	10.033	−0.003	9.442	−0.027	8.889	−0.012

TABLE 4 (*Continued*)

Star	U_{syn}	$U_{obs} - U_{syn}$	B_{syn}	$B_{obs} - B_{syn}$	V_{syn}	$V_{obs} - V_{syn}$	R_{syn}	$R_{obs} - R_{syn}$	I_{syn}	$I_{obs} - I_{syn}$
SA 98-320	11.451	+0.008	10.349	−0.026	9.192	−0.012	8.605	−0.021	8.079	−0.015
SA 98-653	...	...	...	...	...	...	...	...	9.523	−0.001
SA 98-667	8.059	+0.011	8.394	+0.012	8.370	+0.008	8.301	+0.006	8.217	+0.012
SA 98-978	11.284	−0.009	11.179	+0.002	10.572	0	10.235	−0.012	9.916	−0.015
SA 99-6	3.612	−0.022	12.328	−0.025	11.070	−0.016	10.435	−0.033	9.837	−0.012
SA 99-185	10.388	+0.012	9.445	−0.020	8.354	−0.010	7.799	−0.018	7.278	−0.005
SA 99-296	10.890	+0.016	9.656	−0.015	8.460	−0.006	7.861	−0.007	7.322	+0.009
SA 99-358	10.871	+0.019	10.383	−0.002	9.598	+0.007	9.163	+0.010	8.751	+0.016
SA 99-408	10.257	0	10.223	−0.009	9.812	−0.005	9.553	+0.001	9.306	+0.002
SA 99-418	9.289	−0.010	9.429	+0.004	9.469	+0.005	9.471	+0.006	9.489	+0.001
SA 99-438	8.534	−0.016	9.255	−0.012	9.396	+0.002	9.436	+0.021	9.521	+0.018
SA 99-447	9.143	−0.018	9.354	−0.004	9.422	−0.005	9.460	−0.011	9.505	−0.014
SA 100-95	10.111	+0.009	9.750	−0.021	8.927	−0.012	8.492	−0.030	8.058	−0.027
SA 100-162	11.918	+0.005	10.444	−0.018	9.158	−0.008	8.522	−0.021	7.959	−0.012
SA 100-241	10.403	−0.006	10.301	−0.005	10.151	−0.012	10.081	−0.020	9.997	−0.021
SA 100-280	12.291	0	12.292	+0.001	11.803	−0.004	11.510	−0.006	11.221	−0.010
SA 100-606	8.790	+0.028	8.702	−0.009	8.655	−0.014	8.635	−0.020	8.613	−0.020
SA 101-24	10.127	+0.015	9.127	−0.022	8.000	−0.003	7.434	−0.012	6.914	−0.008
SA 101-281	12.844	−0.038	12.405	−0.018	11.582	−0.007	11.122	+0.001	10.706	+0.005
SA 101-282	10.430	+0.011	10.436	−0.005	10.005	−0.003	9.756	−0.014	9.501	−0.019
SA 101-311	8.492	+0.009	8.496	+0.002	8.235	−0.002	8.082	−0.008	7.921	−0.010
SA 101-324	12.031	+0.020	10.914	−0.011	9.750	−0.008	9.174	−0.023	8.643	−0.011
SA 101-333	11.114	−0.007	9.355	−0.035	7.854	−0.019	7.072	−0.032	6.337	−0.026
SA 101-363	10.255	+0.009	10.137	−0.002	9.882	−0.008	9.740	−0.012	9.587	−0.010
SA101-389	10.397	−0.009	10.399	−0.010	9.967	−0.005	9.707	−0.001	9.459	0
SA 102-58	9.470	−0.009	9.452	−0.012	9.387	−0.007	9.342	−0.006	9.336	−0.016
SA 102-276	10.389	−0.011	10.409	−0.007	9.915	−0.005	9.625	−0.006	9.343	−0.008
SA 102-381	8.315	+0.005	8.237	−0.012	7.930	−0.014	7.760	−0.017	7.592	−0.022
SA 102-466	11.218	+0.005	10.319	−0.017	9.255	−0.009	8.701	−0.018	8.184	−0.007
SA 102-472	10.579	+0.008	9.789	−0.021	8.764	−0.010	8.246	−0.020	7.755	−0.012
SA 102-620	12.187	−0.015	11.196	−0.044	10.081	−0.012	9.450	−0.023	8.912	−0.010
SA 102-625	9.477	0	9.454	−0.012	8.907	−0.017	8.605	−0.027	8.304	−0.035
SA 102-1081	10.828	−0.006	10.581	−0.014	9.914	−0.011	9.559	−0.022	9.229	−0.024
SA 103-302	10.181	−0.008	10.239	−0.010	9.868	−0.007	9.639	−0.006	9.403	−0.007
SA 103-462	10.778	−0.014	10.692	−0.017	10.120	−0.009	9.794	−0.007	9.481	0
SA 103-483	8.870	+0.003	8.785	−0.005	8.359	−0.006	8.106	+0.002	7.869	+0.004
SA 104-306[c]	12.447	+0.181	10.876	+0.086	9.315	+0.055	8.501	+0.037	7.737	+0.042
SA 104-337	12.337	−0.026	11.999	−0.024	11.217	−0.010	10.785	−0.012	10.382	−0.007
SA 104-461	10.170	−0.019	10.202	−0.021	9.724	−0.019	9.427	−0.011	9.128	−0.003
SA 104-598	13.610	+0.025	12.585	0	11.448	+0.031	10.832	−0.023	10.295	−0.031
SA 105-28	10.250	+0.004	9.412	−0.028	8.368	−0.023	7.833	−0.021	7.332	−0.005
SA 105-66	9.155	−0.020	9.131	−0.029	8.791	−0.031	8.569	−0.020	8.346	−0.015
SA 105-205	11.748	+0.029	10.193	−0.032	8.811	−0.013	8.064	−0.010	7.365	+0.014
SA 105-214	7.583	−0.003	7.604	−0.014	7.077	−0.015	6.759	−0.010	6.445	−0.007
SA 105-405	11.703	+0.032	9.863	−0.033	8.331	−0.022	7.497	−0.020	6.683	+0.009
SA 105-448	9.457	+0.005	9.437	−0.012	9.192	−0.016	9.035	−0.008	8.869	−0.004
SA 105-663	11.143	+0.016	10.415	−0.012	9.432	−0.006	8.919	−0.015	8.428	−0.005
SA 106-575	12.109	+0.023	10.674	−0.025	9.357	−0.016	8.691	−0.022	8.083	−0.007
SA 106-700	12.678	+0.051	11.170	−0.023	9.798	−0.013	9.082	−0.025	8.419	−0.004
SA 106-834	10.084	−0.003	9.798	−0.009	9.093	−0.005	8.712	−0.003	8.360	−0.008
SA 106-1250	9.986	−0.002	9.180	−0.028	8.144	−0.021	7.617	−0.026	7.115	−0.018
SA 107-35	10.347	+0.016	9.064	−0.010	7.786	−0.007	7.137	−0.021	6.537	−0.007
SA 107-544	9.589	+0.005	9.449	−0.011	9.046	−0.009	8.812	−0.008	8.586	−0.006
SA 107-684	9.136	−0.012	9.067	−0.015	8.442	−0.009	8.085	−0.008	7.733	−0.008

NOTE.—Observed magnitudes taken from Landolt (1983, 1992a, 1992b), Hamuy et al. (1992), and Landolt (1999, private communication).

[a] Possible variable star.

[b] Landolt (1983) lists as possible variable.

[c] Landolt (1983) lists as variable.

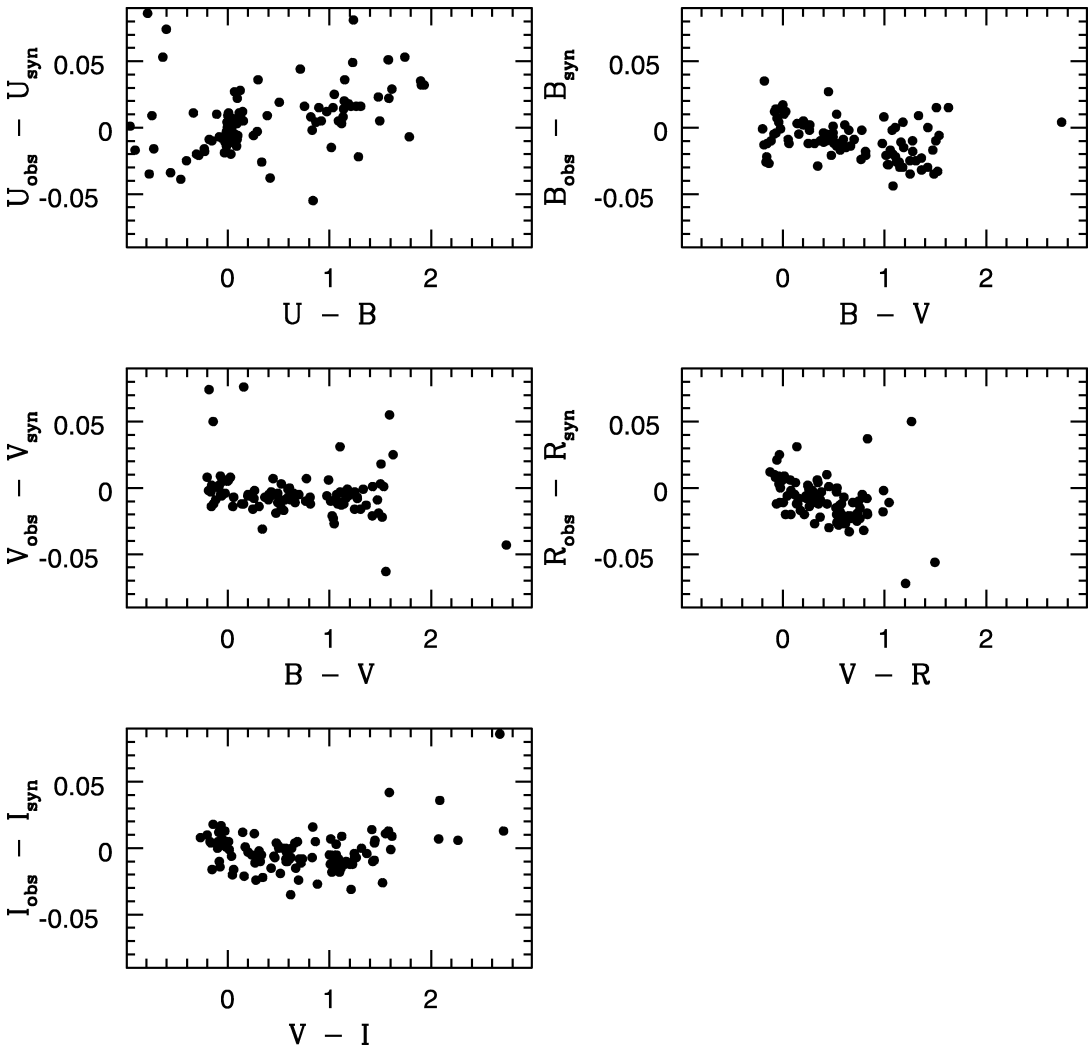

FIG. 4.—Difference between observed and synthetic magnitudes derived using the Bessell passbands (see Fig. 3) as a function of color. Significant outliers are variable stars, identified in Table 4.

TABLE 5
MEAN DIFFERENCES AND STANDARD DEVIATIONS BETWEEN OBSERVED AND SYNTHETIC MAGNITUDES

Filter	Mean Difference	Standard Deviation
U	+0.007	0.023
B	−0.010	0.011
V	−0.006	0.006
R	−0.008	0.010
I	−0.003	0.007

NOTE.—Mean values were determined utilizing an outlier resistance algorithm. Standard deviations were determined using a robust σ algorithm.

TABLE 6
WAVELENGTH SHIFTS APPLIED TO BESSELL PASSBANDS

Passband	Shift (Å)	Color
U	16	Blue
B	8.5	Red
V	6	Red
R	38	Red
I	5	Blue

TABLE 7
NORMALIZED *UBV* STANDARD PASSBANDS

λ	*U*	λ	*B*	λ	*V*
3000	0.000	3600	0.000	4700	0.000
3050	0.034	3700	0.028	4800	0.027
3100	0.113	3800	0.126	4900	0.160
3150	0.236	3900	0.569	5000	0.462
3200	0.376	4000	0.945	5100	0.790
3250	0.525	4100	0.998	5200	0.979
3300	0.662	4200	1.000	5300	1.000
3350	0.770	4300	0.958	5400	0.960
3400	0.855	4400	0.898	5500	0.873
3450	0.913	4500	0.806	5600	0.759
3500	0.958	4600	0.685	5700	0.645
3550	0.983	4700	0.581	5800	0.533
3600	1.000	4800	0.478	5900	0.422
3650	0.997	4900	0.373	6000	0.324
3700	0.987	5000	0.280	6100	0.241
3750	0.947	5200	0.127	6200	0.173
3800	0.851	5300	0.079	6300	0.118
3850	0.713	5400	0.037	6400	0.070
3900	0.526	5500	0.009	6500	0.039
3950	0.334	5600	0.000	6600	0.021
4000	0.175	...	...	6700	0.013
4050	0.080	...	...	6800	0.010
4100	0.035	...	...	6900	0.007
4150	0.010	...	...	7000	0.000
4200	0.000	...	...	...	...

one would apply to the standard passbands in order to increase the color term by 0.01 mag mag^{-1}. In Table 9 the color terms (for example the B band) are in the form $B = \mathrm{ZP} + b_{\mathrm{nat}} + K(B - V)$. Also listed is the color used in each color term.

With the V-band spectrophotometry and dispersion-calibrated spectra, we investigated the LORAL CCD's response for all the nights on which observations were conducted. In Figure 6 we present the difference between standard and synthetic V-band magnitudes as a function of counts in the extracted one-dimensional spectra at the effective V-band wavelength for all observations. We conclude from Figure 6 that the response function of the LORAL CCD was linear to within 2%.

TABLE 8
NORMALIZED *R* AND *I* STANDARD PASSBAND

λ	*R*	λ	*I*
5501.5	−0.052	7001.9	0.000
5511.5	−0.040	7011.9	0.001
5521.5	−0.026	7021.9	0.002
5531.5	−0.012	7031.9	0.003
5541.5	0.003	7041.9	0.004
5551.5	0.019	7051.9	0.005
5561.5	0.037	7061.9	0.007
5571.5	0.056	7071.9	0.010
5581.5	0.077	7081.9	0.014
5591.5	0.100	7091.9	0.021

NOTE.—Table 8 is published in its entirety in the electronic edition of the *PASP*. A portion is shown here for guidance regarding its form and content.

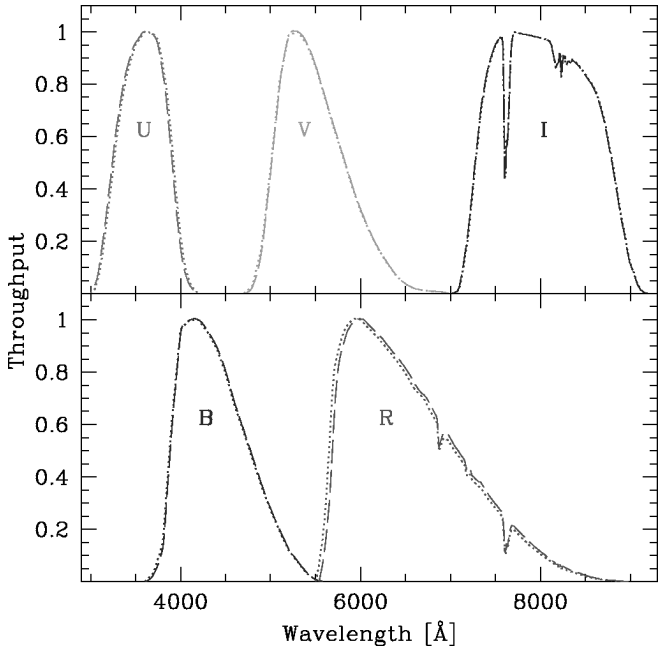

FIG. 5.—Comparison of the Bessell Johnson/Kron-Cousins passbands (*dotted lines*) to our newly modeled passbands (*dashed lines*), which include the shifts listed in Table 6. [*See the electronic edition of PASP for a color version of this figure.*]

4.2. The Sun, Sirius, and Vega

In addition to the selected Landolt standard stars in this work, we have calculated spectrophotometry for the Sun, Sirius, and Vega. As there are no spectrophotometric standards in the infrared comparable to that in the optical, these objects can be useful to accurately characterize the modeled passbands when computing *JHK*-band *S*-corrections (see Krisciunas et al. 2004). Spectra for these objects have been constructed using a combination of empirical and modeled data. The reader is referred to Appendix A in Krisciunas et al. (2003) for a more detailed description of the construction of these spectra; below we provide a brief summary for each of these stars.

Our solar spectrum combines empirical data from Livingston & Wallace (1991), scaled to a solar model from the Kurucz Web site (Kurucz et al. 1984), with physical parameters $T_{\mathrm{eff}} = 5777$ K, $\log g = 4.438$, $v_{\mathrm{micro}} = 1.5$ km s^{-1}, and mixing length/

TABLE 9
FILTER SHIFTS

Passband	Shift (Å)	Color Term
U	12	$(U - B)$
B	7.4	$(B - V)$
V	15.2	$(B - V)$
R	12.4	$(V - R)$
I	40.5	$(V - I)$

NOTE.—All shifts to the red.

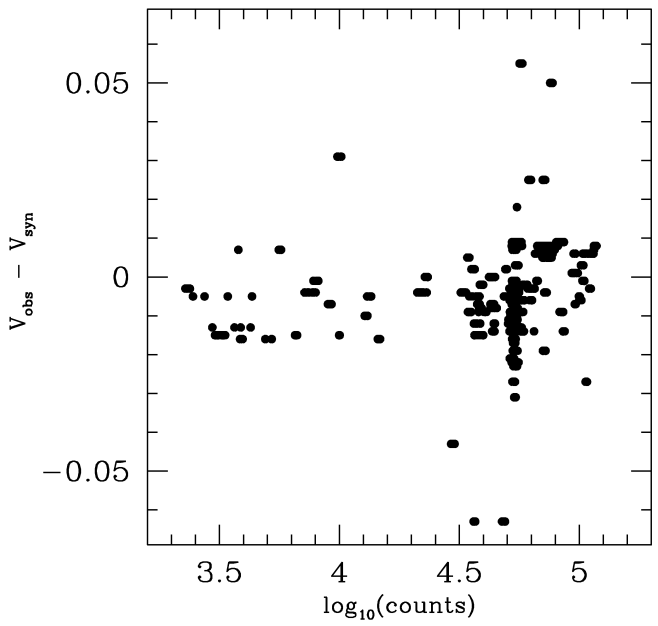

FIG. 6.—*V*-band observed minus synthetic magnitudes vs. photon counts detected by the LORAL CCD at the *V* band's effective wavelength.

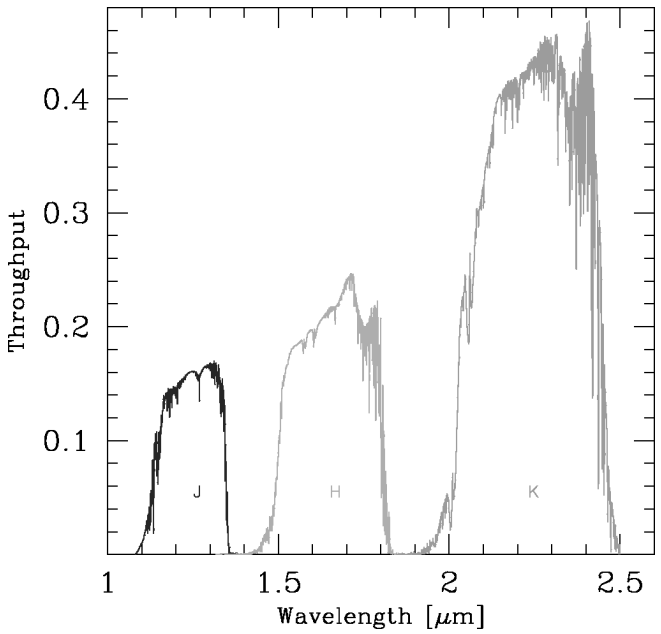

FIG. 7.—Infrared passbands corresponding to Persson et al. (1998) J_s, H, and K_s transmission functions, a NICMOS2 QE, multiple mirror reflections, a Dewar window transmissivity, and an atmospheric line opacity spectrum. [*See the electronic edition of PASP for a color version of this figure.*]

scale height = 1.25. For Vega we have adopted observational data from Hayes (1985). His data were combined with the Kurucz spectrum vega090250000p.asc5, with physical parameters $T_{\rm eff}$ = 9550 K, log g = 3.950, $v_{\rm micro}$ = 2 km s^{-1}, and mixing length/scale height = 0. The Kurucz model was then scaled to match the flux points of Hayes (1985). The Sirius spectrum was constructed using the Kurucz model sir.ascsq5, scaled to force the synthetic *V* magnitude to equal the observed value of −1.430 (Bessell et al. 1998). Each of these spectra were convolved to 2 Å and resampled to 1 Å per pixel.

To compute *UBVRI* synthetic photometry, we employed our newly modeled passbands (shown in Fig. 5) and the zero points listed in Table 3. To calculate *JHK*-band synthetic magnitudes, we constructed instrumental passbands (see Fig. 7), which included information associated with the Las Campanas Observatory's 1 m Henrietta Swope telescope, where the Persson et al. (1998) infrared system was established. This includes Persson et al. J_s, H, and K_s filter transmissivities, a Rockwell NICMOS2 QE response function, two aluminum reflections, a Dewar window transmissivity, multiple reflections associated with optical elements within the C40IRC camera, and an atmospheric line opacity spectrum. Zero points were calculated by forcing the synthetic magnitudes of Vega to equal that of the Elias et al. (1982) CIT photometric system; i.e., J = 0, H = 0, K = 0. The resulting *JHK*-band zero points were −11.954, −11.895, and −12.063, respectively.

Table 10 lists the published photometry (from multiple sources), our synthetic photometry, and the difference between the two in the sense of observed minus synthetic. The difference between Vega's *V*-band observed and synthetic magnitudes shows that our zero points, calculated using the secondary standards from Hamuy et al. (1994), have an associated error of ~0.01 mag. The large differences in the *UB* bands may be due to the difficulty in obtaining accurate measurements of a star as bright as Vega. There is poor agreement for the Sun between *UJHK* observed and synthetic magnitudes. This is also not surprising, considering the difficulty in obtaining precise photometry of a source as bright and extended as the Sun. Some of the large *U*-band difference may be a result of the large variability of both the Sun's flux in the ultraviolet and Earth's atmospheric transmissivity. The differences in the infrared may be attributed to telluric absorption features that were not sufficiently accounted for in our manufactured instrumental passbands. The near-infrared spectrophotometry of Sirius matches well with observed photometry to within 1% or less, while in the optical the difference is on the order of 4% or less.

We thank the anonymous referee for helpful comments. A special thanks goes to Arlo Landolt for providing us with updated values for the spectrophotometric standards. We also acknowledge Mike Bessell, Kevin Krisciunas, Brian Schmidt, Eric Persson, and Fiorella Castelli for helpful discussions on photometry and spectrophotometry. We are grateful to Phil Massey and William Vacca for providing us with their modified version of a Kurucz stellar atmosphere code. We thank Bruno Leibundgut for useful comments on a preliminary draft of this manuscript. M. S. acknowledges financial support from *Hubble Space Telescope* grant GO-07505.02-96A, and the International

TABLE 10
SPECTROPHOTOMETRY OF THE SUN, SIRIUS, AND VEGA

Passband	*U*	*B*	*V*	*R*	*I*	*J*	*H*	*K*	Reference
Sun:									
m_{obs}	−25.947	−26.104	−26.755	−27.118	−27.464	−27.885	−28.219	−28.261	1
m_{syn}	−25.968	−26.105	−26.764	−27.121	−27.456	−27.939	−28.260	−28.307	
$m_{obs} - m_{syn}$	+0.021	+0.001	+0.009	+0.003	−0.008	+0.054	+0.041	+0.046	
Sirius:									
m_{obs}	−1.480	−1.435	−1.430	−1.419	−1.412	−1.385	−1.382	−1.367	2
m_{syn}	−1.438	−1.435	−1.423	−1.390	−1.374	−1.392	−1.381	−1.377	
$m_{obs} - m_{syn}$	−0.042	0	−0.007	−0.029	−0.038	+0.007	−0.001	+0.010	
Vega:									
m_{obs}	+0.025	+0.025	+0.030	+0.039	+0.035	−0.001	0	−0.001	3
m_{syn}	+0.088	+0.003	+0.026	+0.052	+0.045	0	0	0	
$m_{obs} - m_{syn}$	−0.063	+0.022	+0.004	−0.013	−0.010	−0.001	0	−0.001	

REFERENCES—(1) Averaged values from Table A3 of Bessell et al. (1998), referenced from Stebbins & Kron (1957), Colina et al. (1996), and Cayrel de Strobel (1996); (2) Table A2 of Bessell et al. (1998, and references within), *UBRI* averaged values, *JHK* from Table A1 of Cohen et al. (1999); (3) Table A2 of Bessell et al. (1998), *B* averaged value, *JHK* from Table A2 of Cohen et al. (1999).

Max-Planck Research School on Astrophysics. This research has made use of the SIMBAD database, operated at CDS, Strasbourg, France.

REFERENCES

Bessell, M. S. 1983, PASP, 95, 480
———. 1990, PASP, 102, 1181
———. 1999, PASP, 111, 1426
Bessell, M. S., Castelli, F., & Plez, B. 1998, A&A, 337, 321
Candia, P., et al. 2003, PASP, 115, 277
Cayrel de Strobel, G. 1996, A&A Rev., 7, 243
Cohen, M., et al. 1999, AJ, 117, 1864
Colina, L., Bohlin, R. C., & Castelli, F. 1996, AJ, 112, 307
Elias, J. H., Frogel, J. A., Matthews, K., & Neugerbauer, G. 1982, AJ, 87, 1029
Hamuy, M., Suntzeff, N. B., Bravo, J., & Phillips, M. M. 1990, PASP, 102, 888
Hamuy, M., et al. 1992, PASP, 104, 533
———. 1994, PASP, 106, 566
———. 2001, ApJ, 558, 615
Hayes, D. S. 1970, ApJ, 159, 165
———. 1985, in IAU Symp. 111, Calibration of Fundamental Stellar Quantities (Dordrecht: Reidel), 225
Jha, S. 2002, Ph.D. thesis, Harvard Univ.
Krisciunas, K., et al. 2003, AJ, 125, 166
———. 2004, AJ, 127, 1664
Kurucz, R. L., Furenlid, I., & Brault, J. T. L. 1984, Solar Flux Atlas from 296 to 1300 nm (Sunspot: NSO)
Landolt, A. U. 1983, AJ, 88, 439
———. 1992a, AJ, 104, 340
———. 1992b, AJ, 104, 372
Livingston, W., & Wallace, L. 1991, An Atlas of the Solar Spectrum in the Infrared from 1850 to 9000 cm^{-1} (1.1 to 5.4 Microns) (NSO Tech. Rep. 91-001; Tucson: NSO)
Massey, P., et al. 1988, ApJ, 328, 344
Menzies, J. W. 1989, MNRAS, 237, 21
Persson, S. E., Murphy, D. C., Krzeminski, W., Roth, M., & Rieke, M. J. 1998, AJ, 116, 2475
Pignata, G., et al. 2004, MNRAS, 355, 178
Stebbins, J., & Kron, G. E. 1957, ApJ, 126, 226
Stritzinger, M., et al. 2002, AJ, 124, 2100
Suntzeff, N. B. 2000, in AIP Conf. Proc. 522, Cosmic Explosions, ed. S. S. Holt & W. W. Zhang (New York: AIP), 65
Suntzeff, N. B., Hamuy, M., Martin, G., Gómez, A., & González, R. 1988, AJ, 96, 1864
Suntzeff, N. B., et al. 1999, AJ, 117, 1175
Taylor, B. J. 1984, ApJS, 54, 259